名古屋大学博物館報告
Bull. Nagoya Univ. Museum
No. 33, 15–30, 2018
DOI: 10.18999/bulnum.033.02

Geochemistry of the Permian–Triassic volcano-plutonic rocks in the Oyut-uul area, northeast of Darkhan, Mongolia —Magmatism at southern margin of Siberian continent—

Kazuhiro TSUKADA[1]*, Nemekhbayar PUREVSUREN[2], Manchuk NURAMKHAAN[2], Onon GANTUMUR[3], Hitoshi HASEGAWA[4], and Koshi YAMAMOTO[3]

[1] The Nagoya University Museum, Nagoya 464-8601, Japan
[2] School of Geology and Mining, Mongolian University of Science and Technology, Ulaanbaatar, Mongolia
[3] Graduate School of Environmental Studies, Nagoya University, Nagoya 464-8601, Japan
[4] Graduate School of Science, Kochi University, Kochi 780-8520, Japan

*Corresponding author: Tel.: +81-52-789-5768; fax: +81-52-789-5896
E-mail address: tsukada@num.nagoya-u.ac.jp (K. Tsukada)

Abstract

The geochemistry of the Late Paleozoic–Early Mesozoic volcano-plutonic rocks of northern Mongolia is a key factor to understand the subduction-related magmatism at the southern margin of "Siberian continent (Siberian craton + accreted geologic units)." Many studies have been carried out in the volcano-plutonic rocks; however, fundamental questions on its detail petrogenesis still remain unanswered. This paper describes the geochemistry of the Permian–Triassic volcano-plutonic rocks at the Oyut-uul area, northeast of Darkhan City, Mongolia. The mid-ocean ridge basalt (MORB)-normalized multi-element pattern (spidergram) for the examined rocks shows an enrichment of large-ion lithophile elements (LILE) against high-field-strength elements (HFSE) and rare earth elements (REE), with clear negative Nb anomaly to suggest an arc-related igneous activity. The most data are plotted in the calc-alkaline field in the SiO_2 vs. FeO*/MgO diagram. It is, thus, concluded that the examined rocks are of calc-alkaline series formed at an arc environment. The present samples, 53–78 wt.% SiO_2, high Al_2O_3 and Sr concentrations, high La/Yb ratio, and low K_2O/Na_2O ratio, have adakitic nature derived from oceanic slab-melt. They are quite similar to the marginal facies of the Kitakami adakitic granite of Japan in Sr/Y-Y relationship, MgO concentration, spidergram, and REE chondrite-normalized pattern. It is considered that the marginal facies of the Kitakami adakitic granite was resulted from interaction between the slab-melt and mantle peridotite/lower crustal amphibolite during their ascent. The Oyut-uul rocks might be also derived from oceanic slab-melt interacted with mantle peridotite/lower crustal amphibolite.

Key word: Late Paleozoic–Early Mesozoic; adakites; southern margin of Siberian continent; Mongolia

Introduction

The development process of the Central Asian Orogenic belt (CAOB, Fig. 1), which lies among Siberian craton, North China block, Tarim block, and East European craton (e.g. Sengör et al., 1993), is important to understand tectonic history of Eurasian continent (e.g. Kovalenko et al., 2004). The CAOB is generally considered to have been formed by subduction-accretion process of oceanic plate, volcanic arc magmatism, and collisions of continental fragments during the amalgamation of these cratons and blocks. Geological information of Mongolia, between the North China block and the Siberian craton, offers a key to understanding of the Paleo–Mesozoic tectonics of the southern margin of "Siberian continent (Siberian craton + accreted geologic units)" at southern

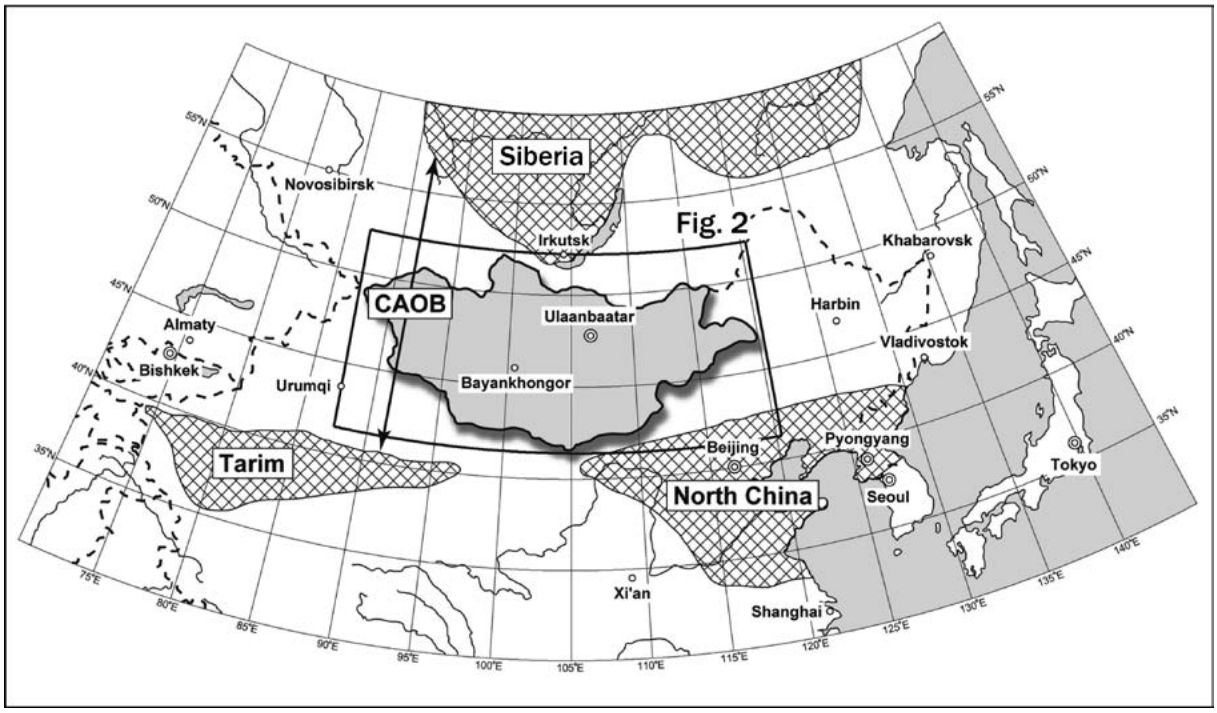

Fig. 1 Index map (modified from Kurihara et al., 2008). CAOB: Central Asia Orogenic belt, Siberia: Siberian craton, North China: North China block, Tarim: Tarim block.

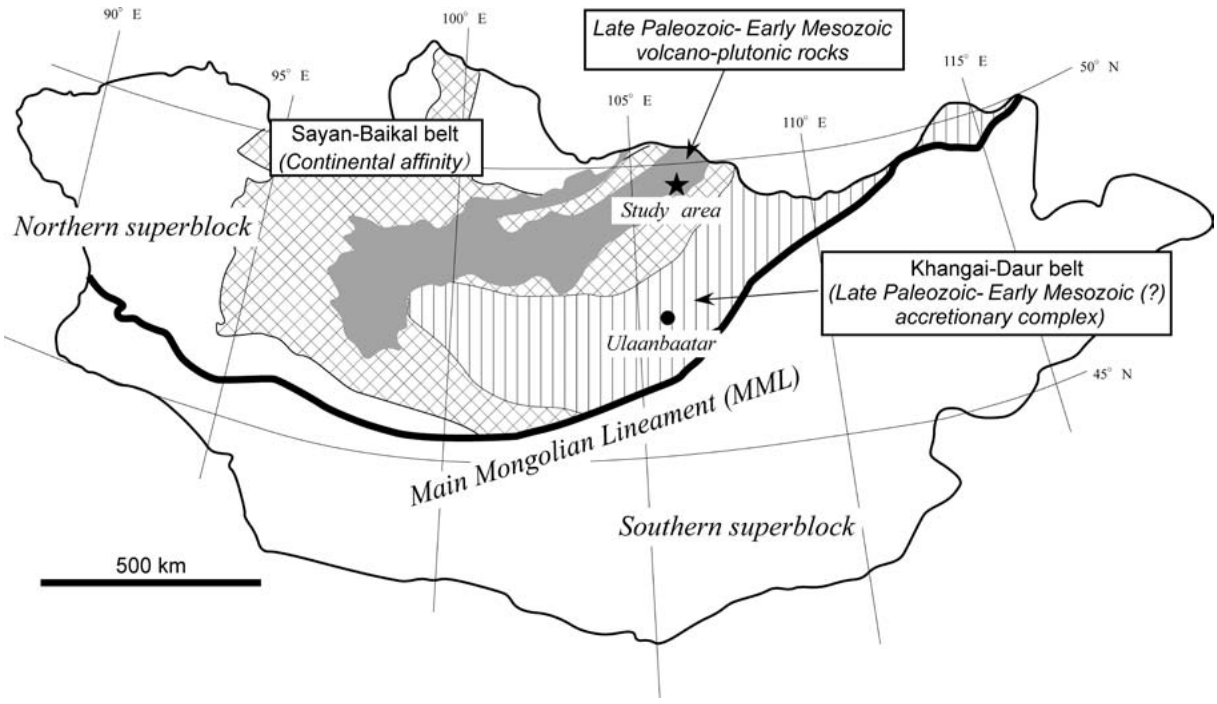

Fig. 2 Simplified tectonic division of Mongolia (modified from Badarch et al. [2002] and Tomurtogoo [2003]).

CAOB, and general features of the Khangai-Daur and Sayan-Baikal belts, a major constituent of the northern Mongolia, was substantially established (e.g. Badarch et al., 2002; Kurihara et al., 2008; Onon, 2017 MS; Onon and Tsukada, 2017; Tomurtogoo, 2003, Fig. 2). Kurihara et al. (2008) revealed that a part of the Khangai-Daur belt is composed of Late Paleozoic accretionary complex that formed by subduction of previous oceanic plate of the Mongol-Okhotsk Ocean. Onon (2017 MS) refined the tectonic division of these belts, i.e. Late Paleozoic–Early Mesozoic (?) accretionary complex of the Khangai-Daur belt and continental affinity (Precambrian–Early Paleozoic basement and intrusive rocks) of the Sayan-Baikal belt (Fig. 2), and described a late Paleozoic subduction-related "doubly-vergent structure" within them.

Although the subduction-related Late Paleozoic–Early Mesozoic volcano-plutonic rocks in the southern margin of the Sayan-Baikal belt is an important factor to reveal the arc system along the Siberian continental margin, little attention has been made at its petrogenesis (Fig. 2). This paper describes geochemistry of the Permian–Triassic volcanic and plutonic rocks in the Oyut-uul area, northeast of Darkhan City, Mongolia, and makes preliminary discussion on its petrogenesis (Fig. 2).

Geological framework

Mongolia is geologically divided into the Northern and Southern superblocks by the Main Mongolian Lineament (MML; Tomurtogoo, 2003, Fig. 2). The Northern superblock, i.e. southern margin of the "Siberian continent," is largely occupied by the Late Paleozoic–Early Mesozoic (?) accretionary complex of the Khangai-Daur belt and the continental affinity of the Sayan-Baikal belt (Petrov et al., 2014; Onon, 2017 MS; Onon and Tsukada, 2017, Fig. 2). The Khangai-Daur belt is composed mainly of sandstone and mudstone with minor amounts of radiolarian chert, siliceous mudstone, oceanic island basalts, and limestone (e.g. Badarch et al., 2002; Tomurtogoo, 2003; Kurihara et al., 2008; Takeuchi et al., 2012; Tsukada et al., 2013). The rocks of the belt are intruded by Permian–Jurassic granitic rocks, and are partly metamorphosed and sheared. The Sayan-Baikal belt is mainly composed of Precambrian–Cambrian metamorphic rocks and limestone, Precambrian–Ordovician granitic rocks, and Silurian–Carboniferous limestone, volcanic rocks and clastic rocks. These rocks are covered/intruded by the Late Paleozoic–Early Mesozoic volcano-plutonic rocks, then are intruded by Mesozoic granitic rocks (e.g. Onon, 2017 MS).

The study area, in the Sayan-Baikal belt, exposes the Late Paleozoic–Early Mesozoic volcano-plutonic rocks. The rocks in the area are assigned to the Permian Khanui Group and the Permian–Triassic Selenge complex (Gombosuren and Batchuluun, 1994, Fig. 3). The Khanui Group here is composed mainly of andesite–dacite lava and pyroclastic rocks. The lava is fine to coarse-grained, and has intersertal, subophitic/ophitic or porphyritic textures. The main constituent of the rock is plagioclase, and next in abundance is clinopyroxene, then hornblende and its pseudomorph replaced by chlorite. In the lava showing porphyritic texture, idiomorphic or hypidiomorphic laths of plagioclase, more than 1 mm in major axis, lie in groundmass composed of smaller plagioclase, clinopyroxene, and interstitial chloritic material. It was partly altered to the extent that some of the minerals, except for plagioclase and clinopyroxene, are replaced by secondary minerals such as chlorite and opaque minerals. It is considered that the Khanui Group is intruded by the rocks of the Selenge complex (Gombosuren and Batchuluun, 1994). The Selenge complex in this area is largely made up of diorite–granodiorite–granite, which is intruded by numerous andesite/dacite/diorite dikes. The diorite–granodiorite–granite is generally medium- to coarse-grained, holocrystalline, and the majority of the plagioclase and quartz crystals are idiomorphic, fresh, and clear. Biotite is commonly included in the diorite–granodiorite–granite. The dike rock, hemicrystalline, porphyritic/aphyric, is

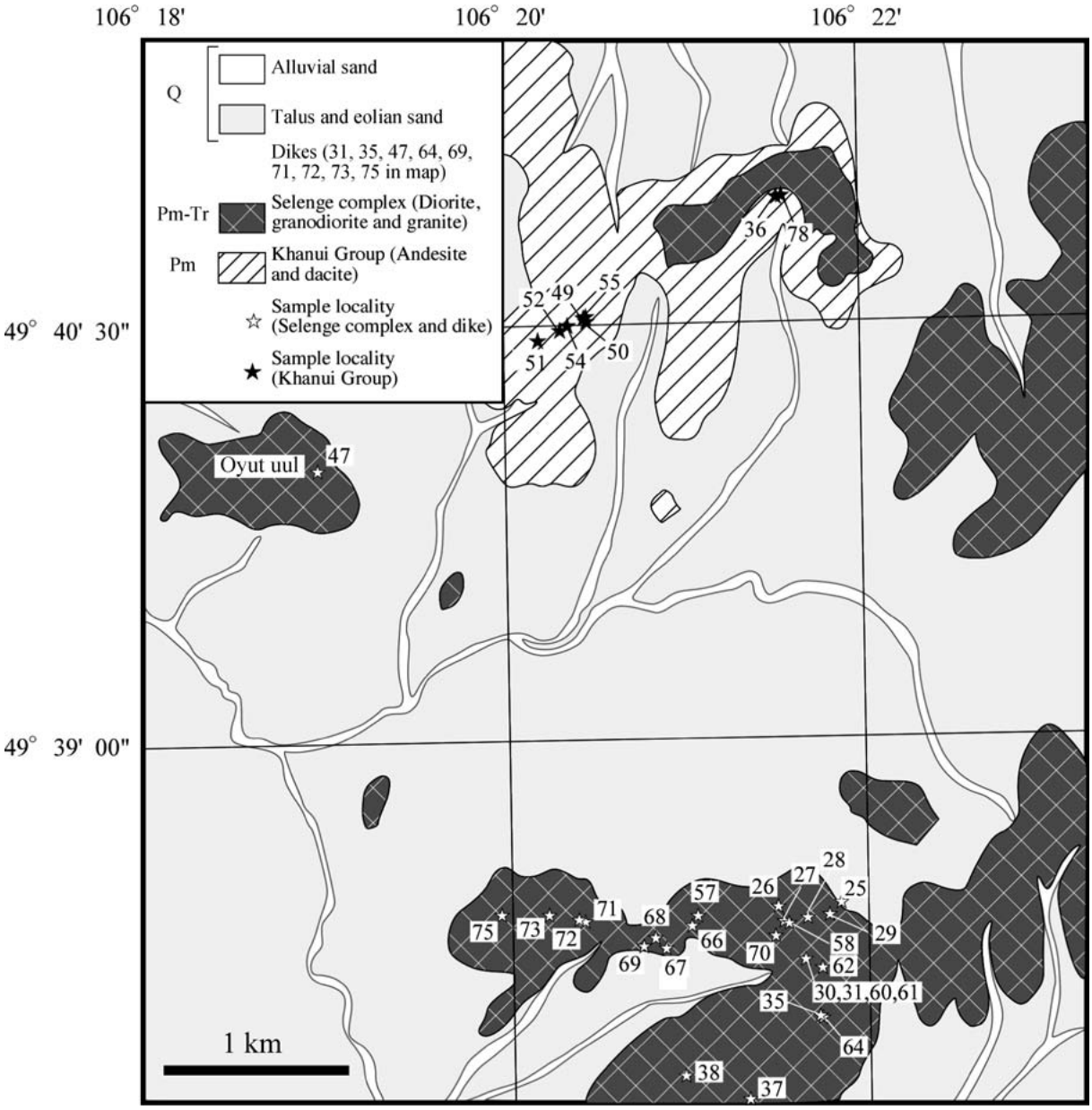

Fig. 3 Geologic map of the study area after Gombosuren and Batchuluun (1994). Sampling localities are also shown. Pm: Permian, Tr: Triassic, Q: Quaternary.

composed of idiomorphic to hypidiomorphic laths of plagioclase and smaller interstitial patches of plagioclase and chloritic material. The Khanui Group yields Permian plant fossils (Mossakovsky and Tomurtogoo, 1976). The Selenge complex gives ^{40}Ar-^{39}Ar ages of 258.6 ± 3.3 Ma and 247 ± 3.7 Ma, and K-Ar ages of 250–210 Ma (Koval et al., 1982; Gerel and Munkhtsengel, 2005; Munkhtsengel et al., 2007; Sotnikov et al., 1985).

Whole-rock chemistry

Methodology

Thirty-five samples (nine from andesite–dacite lava of the Khanui Group, seventeen from the diorite–granodiorite–granite of the Selenge complex, and nine from the andesite/dacite/diorite dike) were taken for

analysis (Fig. 3). After coarse crushing, veins and altered parts of the samples were carefully excluded using × 20 hand loupe. Each analysis sample weighed > 500 g. Major element compositions and Co, Zr, Nb, and Th were determined by X-ray fluorescence (XRF; Rigaku Primus II ZSX equipped with Rh X-ray tube, 50 kV, 60 mA), and other trace elements and rare earth elements (REE) were analyzed by Inductively Coupled Plasma Mass Spectrometry (Quadrupole type ICP-MS; Agilent 7700x) installed at Nagoya University. In the XRF analysis, glass beads were prepared by fusing mixtures of 1.5 g of powdered sample with 6.0 g of lithium tetraborate. Calibration was carried out using standard rock samples issued by the Geological Survey of Japan (GSJ) and the composite standards prepared by Yamamoto and Morishita (1997). Analytical precision of major elements was estimated to be < 1% for Si and about 3% for other elements, except for CaO, MgO and Na_2O, whose analytical precision is > 3% when the measured level is < 0.1% (Takebe and Yamamoto, 2003), and that for trace elements was estimated to be less than 10% (Yamamoto and Morishita, 1997). The other trace elements and REE were determined based on the method that described by Yamamoto et al. (2005). About 30 mg of each sample was digested with a mixed solution of HF-$HClO_4$ (2:1 by volume) at 150 ˚C. After complete evaporation of the acids, 2 ml of 1.7 N-HCl was added to dissolve the cake. The residue was separated by centrifugation at 12000 rpm with a 2 ml polypropylene tube. The supernatant after centrifugation was transferred to another 10 ml Teflon beaker. The residue was then fused with HF-$HClO_4$ (2:1 by volume) again at 150 ˚C. The fused cake was dissolved with about 2 ml 1.7 N-HCl by mild heating, and the solution was centrifuged at 12000 rpm. In most cases, no residue was recognized after centrifugation. The HCl solution was evaporated to dryness and then the fused cake was re-dissolved in 2%-HNO_3 solution and determined by ICP-MS. Indium and Bi were used for tracing ICP sensitivities; the In and Bi concentrations were mostly same throughout the analysis. The oxide generation factor (LnO/Ln) was determined for each 20 ppb solution and used for REE analytical data correction. Analytical accuracy was checked by repeated analysis of standard samples which were prepared from JB-1a (basalt: GSJ geochemical reference sample) and BCR-1 (basalt: geochemical reference materials of the US Geological Survey). In the ICP-MS analysis, the correlation coefficients (R-value) of each element, calculated for five standard samples, were > 0.9999 and the concentration relative standard deviation of the data were mostly less than 3 %. The whole-rock compositions of the samples are listed in Table 1, and are displayed on variation diagrams for selected elements against SiO_2 in Fig. 4.

Geochemical description of the samples

The SiO_2 concentration is between 58–67 wt.% in the lava of the Khanui Group, 53–78 wt.% in the diorite–granodiorite–granite of the Selenge complex, and 53–68 wt.% in the andesite/dacite/diorite dike. The loss of ignition of the samples is mostly less than 4 wt.% (Table 1). The samples are nearly identical to each other in their concentration of the following elements: Al_2O_3 ca. 16 wt.%; Na_2O ca. 4 wt.%; Zr ca. 190 ppm; Nb ca. 6 ppm (Table 1, Fig. 4). K_2O, Rb, and Ba show an increasing trend, and Fe_2O_3*, TiO_2, MnO, CaO, MgO, P_2O_5, Co, Cr, Sr and Y show a decreasing trend against increasing of SiO_2 in the variation diagram (Fig. 4). The rocks are assigned to medium-potassium series (Fig. 4). The samples have FeO*/MgO ratio ranging from 1.1 to 8.8, and MgO concentration ranges from 0.2 to 4.0. The samples have high Sr concentration (172–1470 ppm, avg. 557 ppm), and La/Yb ratio ranges from 5 to 19. The MORB-normalized multi-element concentration diagrams (hereinafter called "spidergram") show reducing trend, and distinctive negative Nb and Cr anomalies and positive K and Pb anomalies (Fig. 5). The chondrite-normalized REE patterns show reducing trend, that is, enriched in Light-REE and depleted in Heavy-REE (Fig. 6).

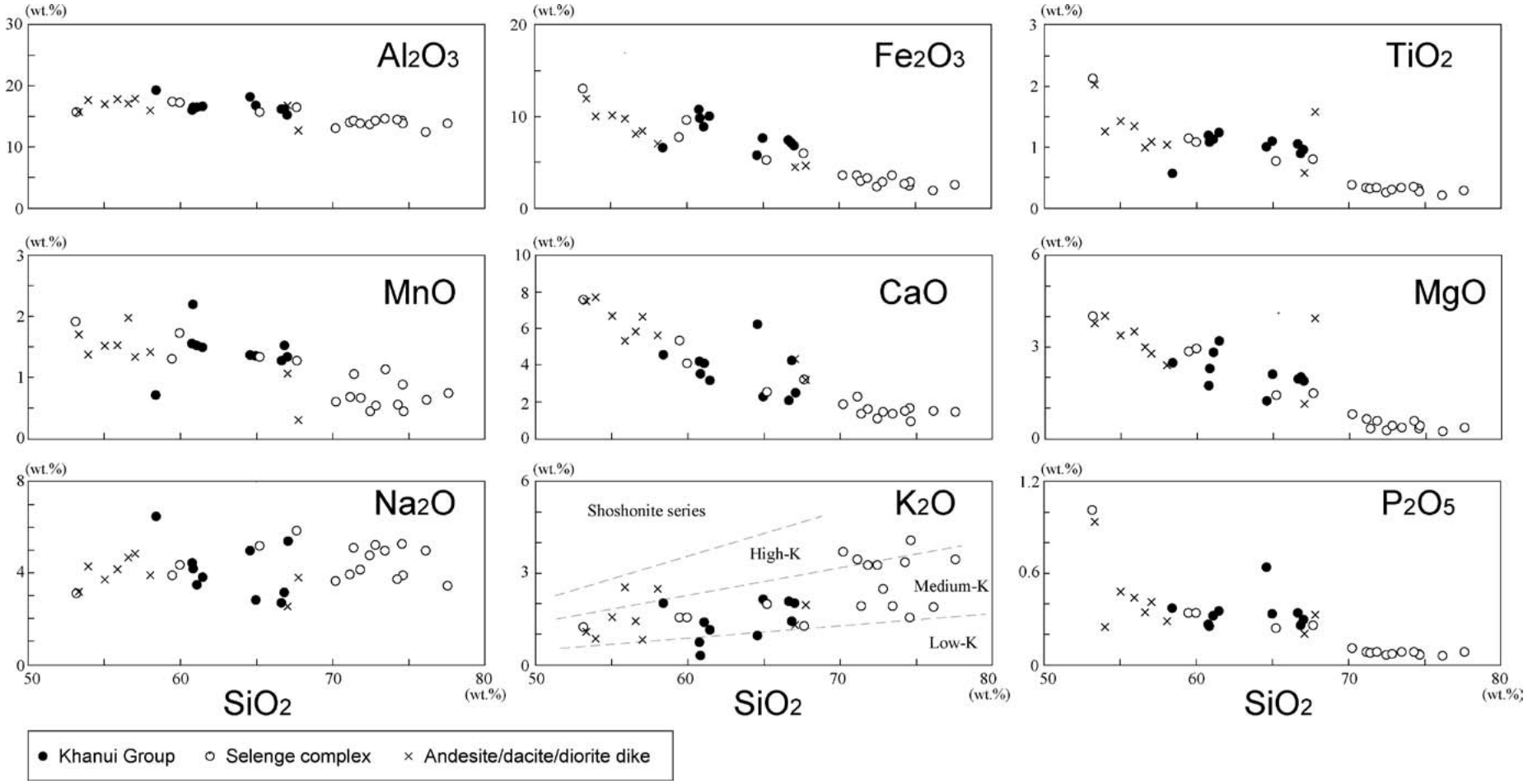

Fig. 4 Variation diagrams of the selected major oxides and trace elements against SiO_2. The data from the Khanui Group, Selenge complex, and andesite/dacite/diorite dike make a clear liner trend together in the most major elements and Co, Sr, Y, and Zr.

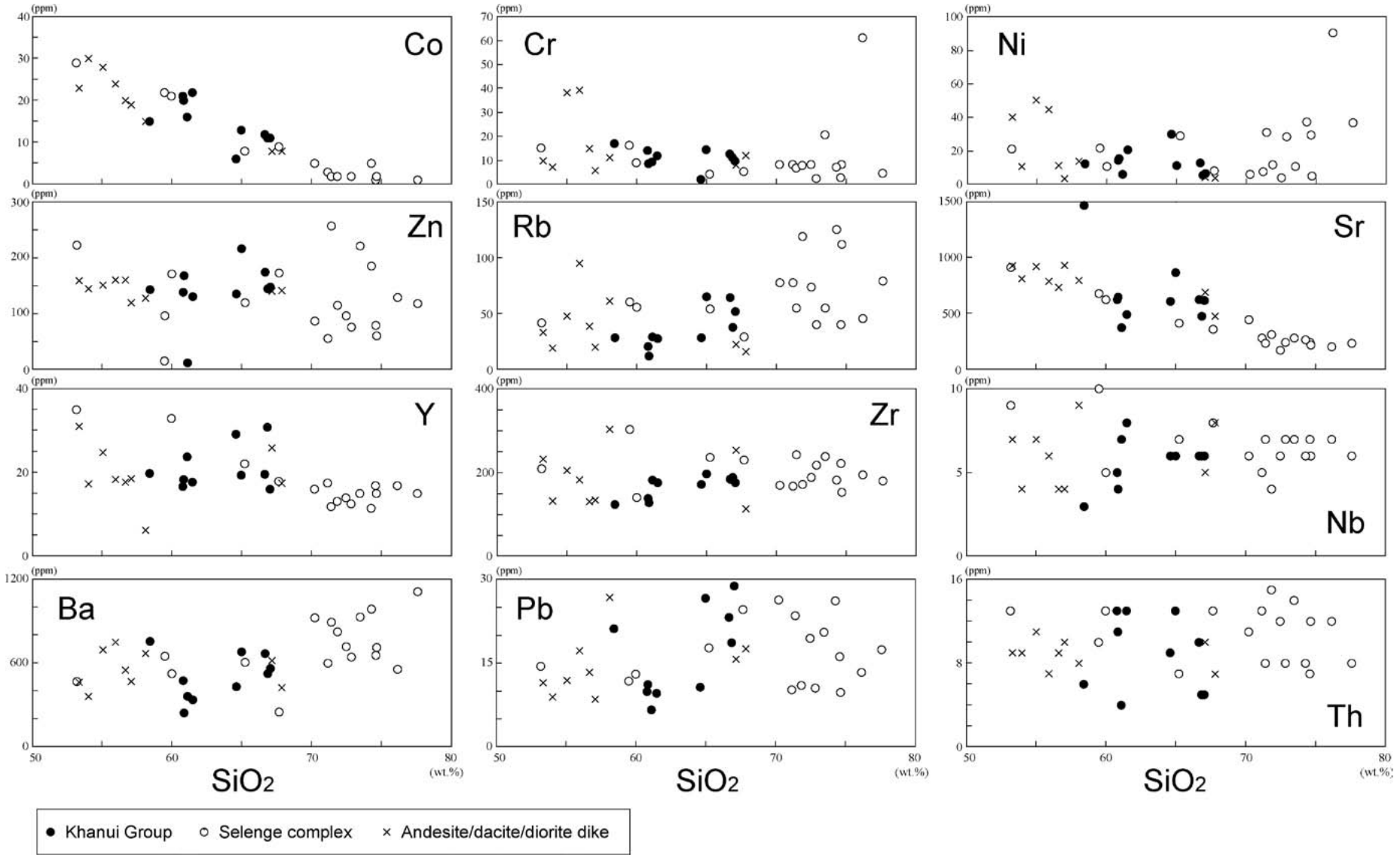
Co
Cr
Ni
Zn
Rb
Sr
Y
Zr
Nb
Ba
Pb
Th
(ppm)
SiO2
(wt.%)
Khanui Group
Selenge complex
Andesite/dacite/diorite dike

Fig. 4 (Cont.)

Table 1 Whole-rock chemical composition displayed to 3 significant digits, except for MnO, P_2O_5, Co, Zr, Nb, and Th.

	Khanui Group									Selenge complex																		Andesite/dacite/diorite dike								
	andesite–dacite lava									Diorite–granodiorite–granite																										
No	40	43	49	50	51	52	54	55	78	25	26	27	28	29	30	37	38	57	58	60	61	62	66	67	68	70	31	35	47	64	69	71	72	73	75
Major element (wt %)																																			
SiO_2	61.0	67.0	66.8	58.4	61.5	60.8	60.8	64.9	66.6	59.4	74.2	71.4	77.5	76.1	65.2	74.5	72.8	71.8	73.5	67.6	53.1	59.9	71.1	70.2	72.4	74.6	53.3	55.9	67.8	55.0	67.1	53.9	57.0	58.0	56.6
Al_2O_3	16.6	15.3	16.2	19.4	16.8	16.1	16.5	16.9	16.3	17.4	14.6	14.4	13.9	12.5	15.8	14.3	14.4	14.0	14.7	16.6	15.8	17.4	14.2	13.1	13.7	13.9	15.8	17.8	12.9	17.0	16.9	17.7	18.0	16.2	17.2
Fe_2O_3*	9.00	6.89	7.22	6.67	10.1	10.8	9.86	7.72	7.54	7.78	2.77	3.04	2.62	2.01	5.31	2.54	2.94	3.30	3.70	6.04	13.1	9.66	3.63	3.69	2.44	2.91	12.0	9.85	4.67	10.2	4.55	10.1	8.41	7.03	8.12
TiO_2	1.15	0.971	0.912	0.579	1.26	1.21	1.09	1.11	1.07	1.16	0.364	0.330	0.295	0.219	0.782	0.332	0.312	0.343	0.347	0.815	2.14	1.10	0.342	0.394	0.269	0.288	2.05	1.36	1.60	1.43	0.585	1.27	1.09	1.04	1.00
MnO	0.15	0.14	0.15	0.07	0.15	0.16	0.22	0.14	0.13	0.13	0.06	0.11	0.08	0.06	0.13	0.09	0.06	0.07	0.11	0.13	0.19	0.17	0.07	0.06	0.05	0.05	0.17	0.15	0.03	0.15	0.11	0.14	0.14	0.14	0.20
CaO	4.14	2.55	4.25	4.57	3.20	4.21	3.56	2.32	2.11	5.35	1.53	1.37	1.46	1.52	2.55	1.65	1.48	1.64	1.36	3.24	7.62	4.14	2.28	1.90	1.12	0.929	7.57	5.31	3.21	6.75	4.31	7.74	6.66	5.61	5.83
MgO	2.85	1.92	2.05	2.50	3.23	1.75	2.31	2.13	1.98	2.87	0.608	0.355	0.365	0.247	1.43	0.342	0.454	0.605	0.377	1.50	4.03	2.97	0.67	0.812	0.285	0.436	3.80	3.52	3.97	3.37	1.12	4.05	2.77	2.41	3.02
Na_2O	3.51	2.59	3.16	6.50	3.83	4.48	4.20	2.84	2.70	3.91	3.76	5.12	3.46	4.99	5.22	5.30	5.26	4.18	5.01	5.88	3.13	4.37	3.96	3.66	4.80	3.93	3.18	4.17	3.80	3.77	5.43	4.28	4.83	3.94	4.67
K_2O	1.42	2.04	1.45	2.04	1.15	0.747	0.328	2.15	2.11	1.58	3.36	1.94	3.47	1.92	2.01	1.58	2.52	3.29	1.95	1.27	1.27	1.57	3.46	3.72	3.29	4.10	1.10	2.52	1.96	1.56	1.30	0.857	0.860	2.51	1.46
P_2O_5	0.32	0.30	0.27	0.38	0.36	0.27	0.26	0.34	0.35	0.35	0.09	0.08	0.09	0.07	0.24	0.07	0.07	0.09	0.09	0.26	1.02	0.34	0.09	0.11	0.07	0.07	0.94	0.45	0.33	0.48	0.22	0.25	0.41	0.30	0.35
Total	100.2	99.6	102.5	101.1	101.6	100.5	99.2	100.6	101.0	100.0	101.3	97.8	103.2	99.6	98.7	100.8	100.3	99.3	101.1	103.3	101.4	100.5	99.8	97.7	98.5	101.2	100.0	101.0	98.7	99.8	101.6	100.4	100.1	97.2	97.4
LOI	1.21	3.12	2.97	1.66	4.19	3.18	4.11	3.36	3.27	3.10	1.58	1.23	1.50	1.62	1.89	1.46	0.973	1.06	0.996	3.22	2.22	2.06	0.906	1.04	0.665	0.988	2.69	2.05	0.808	2.11	1.51	1.18	1.08	1.87	1.68
Trace element (ppm)																																			
Cr	9.39	9.78	11.5	17.1	11.9	14.4	8.89	14.6	13.0	16.4	7.17	7.10	4.61	61.2	4.30	3.13	2.60	8.00	20.8	5.43	15.3	9.26	8.27	8.38	8.56	8.26	9.93	39.6	12.0	38.4	8.30	7.47	5.79	11.4	15.1
Co**	16	11	11	15	22	21	20	13	12	22	5	2	1	b.d.l	8	1	2	2	b.d.l	9	29	21	3	5	b.d.l	2	23	24	8	28	8	30	19	15	20
Ni	6.21	6.62	5.90	12.4	21.1	14.6	15.5	11.3	13.0	22.1	37.4	31.4	37.0	90.5	29.3	29.6	28.5	11.9	10.9	8.35	21.3	10.9	8.10	6.10	4.17	5.28	40.2	44.9	4.15	50.5	4.76	10.9	3.63	14.3	11.6
Zn	12.1	148	145	144	132	139	169	217	175	97.1	186	259	120	130	120	79.6	77.0	116	222	174	224	173	57.1	87.8	97.3	61.0	159	161	143	152	141	146	120	129	162
Rb	30.1	52.1	38.2	28.9	28.1	20.9	12.8	65.8	64.6	60.9	126	55.3	79.5	45.9	54.5	40.6	41.1	119	55.2	30.0	42.7	56.3	78.0	78.0	74.0	113	33.4	95.7	16.2	48.8	23.1	19.9	20.8	62.1	38.8
Sr	379	616	481	1470	496	622	653	868	627	677	269	237	238	207	414	243	245	316	282	363	912	629	283	443	172	220	919	792	481	923	692	811	930	798	732
Y	23.7	16.2	30.9	19.8	17.7	16.8	18.4	19.4	19.7	2.04	11.4	11.8	14.9	16.9	22.1	16.9	12.5	13.2	15.1	17.9	35.1	33.0	17.6	16.2	14.1	14.9	31.1	18.3	17.6	24.9	25.8	17.2	18.5	6.19	17.6
Zr**	184	177	190	125	177	139	129	198	185	305	184	244	182	197	238	224	220	173	240	231	211	142	169	171	189	154	233	184	115	206	254	133	136	304	132
Nb**	7	6	6	3	8	5	4	6	6	10	6	7	6	7	7	7	7	4	7	8	9	5	5	6	6	6	7	6	8	7	5	4	4	9	4
Ba	364	566	526	760	338	478	245	684	668	648	987	896	1120	560	606	658	645	829	933	250	472	528	603	929	717	715	461	752	423	696	619	366	472	669	553
Pb	6.66	28.9	18.8	21.3	9.64	10.1	11.3	26.7	23.3	11.9	26.2	23.7	17.5	13.5	17.9	16.2	10.7	11.1	20.7	24.8	14.6	13.2	10.3	26.5	19.5	9.94	11.6	17.3	17.6	12.1	15.7	9.11	8.57	26.9	13.5
Th**	4	5	5	6	13	13	11	13	10	10	8	8	8	12	7	7	8	15	14	13	13	13	13	11	12	12	9	7	7	11	10	9	10	8	9
Rare earth element (ppm)																																			
La	N/A	N/A	18.7	15.1	19.7	15.6	13.7	23.0	N/A	N/A	17.7	19.7	18.4	N/A	25.1	26.1	22.7	19.3	N/A	N/A	N/A	N/A	N/A	N/A	18.0	N/A	N/A	20.6	N/A	24.1	N/A	12.4	18.3	N/A	N/A
Ce	N/A	N/A	43.5	36.9	44.3	31.7	28.1	47.2	N/A	N/A	32.2	36.6	32.7	N/A	48.9	49.0	42.2	35.5	N/A	N/A	N/A	N/A	N/A	N/A	35.5	N/A	N/A	46.5	N/A	53.1	N/A	35.5	45.6	N/A	N/A
Pr	N/A	N/A	5.75	4.47	6.20	4.96	4.35	6.63	N/A	N/A	4.41	5.45	4.59	N/A	6.63	6.14	5.45	4.50	N/A	N/A	N/A	N/A	N/A	N/A	4.04	N/A	N/A	6.57	N/A	7.52	N/A	4.73	6.17	N/A	N/A
Nd	N/A	N/A	24.9	20.0	26.3	22.5	21.3	29.0	N/A	N/A	16.7	20.6	17.7	N/A	27.8	24.1	21.6	17.3	N/A	N/A	N/A	N/A	N/A	N/A	15.1	N/A	N/A	29.5	N/A	33.9	N/A	22.9	28.8	N/A	N/A
Sm	N/A	N/A	4.88	5.64	5.19	5.17	5.12	4.21	N/A	N/A	6.39	3.95	4.23	N/A	3.64	5.56	5.36	5.65	N/A	N/A	N/A	N/A	N/A	N/A	3.37	N/A	N/A	5.59	N/A	4.75	N/A	5.39	5.70	N/A	N/A
Eu	N/A	N/A	1.45	1.59	1.78	1.70	1.56	1.50	N/A	N/A	1.53	0.860	1.41	N/A	0.674	1.51	1.24	1.64	N/A	N/A	N/A	N/A	N/A	N/A	1.22	N/A	N/A	1.74	N/A	1.47	N/A	1.68	1.73	N/A	N/A
Gd	N/A	N/A	4.72	5.38	5.65	6.05	5.27	4.87	N/A	N/A	6.03	3.67	4.23	N/A	3.64	4.82	4.63	6.13	N/A	N/A	N/A	N/A	N/A	N/A	3.17	N/A	N/A	5.68	N/A	4.99	N/A	5.23	5.68	N/A	N/A
Tb	N/A	N/A	0.699	0.770	0.650	0.965	0.715	0.776	N/A	N/A	0.793	0.492	0.620	N/A	0.427	0.655	0.654	0.856	N/A	N/A	N/A	N/A	N/A	N/A	0.421	N/A	N/A	0.778	N/A	0.702	N/A	0.796	0.881	N/A	N/A
Dy	N/A	N/A	4.43	4.77	3.05	5.76	4.15	4.43	N/A	N/A	4.36	2.97	3.62	N/A	3.26	3.62	4.04	5.32	N/A	N/A	N/A	N/A	N/A	N/A	2.25	N/A	N/A	5.03	N/A	4.37	N/A	4.70	4.87	N/A	N/A
Ho	N/A	N/A	0.883	0.944	0.562	1.09	0.792	0.757	N/A	N/A	0.861	0.657	0.728	N/A	0.648	0.703	0.832	0.983	N/A	N/A	N/A	N/A	N/A	N/A	0.489	N/A	N/A	0.984	N/A	0.765	N/A	0.862	1.00	N/A	N/A
Er	N/A	N/A	2.58	2.91	1.61	3.26	2.84	2.83	N/A	N/A	2.33	1.87	2.45	N/A	1.86	1.89	2.38	3.44	N/A	N/A	N/A	N/A	N/A	N/A	1.38	N/A	N/A	3.01	N/A	2.91	N/A	2.66	3.00	N/A	N/A
Tm	N/A	N/A	0.403	0.421	0.223	0.510	0.395	0.389	N/A	N/A	0.338	0.296	0.329	N/A	0.311	0.262	0.346	0.437	N/A	N/A	N/A	N/A	N/A	N/A	0.187	N/A	N/A	0.424	N/A	0.403	N/A	0.428	0.462	N/A	N/A
Yb	N/A	N/A	2.11	2.36	1.35	3.28	2.64	2.58	N/A	N/A	1.98	1.88	2.22	N/A	2.16	1.50	2.40	3.03	N/A	N/A	N/A	N/A	N/A	N/A	1.12	N/A	N/A	2.30	N/A	2.69	N/A	2.27	2.50	N/A	N/A
Lu	N/A	N/A	0.306	0.264	0.185	0.430	0.371	0.354	N/A	N/A	0.253	0.283	0.336	N/A	0.284	0.253	0.389	0.431	N/A	N/A	N/A	N/A	N/A	N/A	0.213	N/A	N/A	0.278	N/A	0.416	N/A	0.407	0.437	N/A	N/A

Fe_2O_3: total iron as Fe2O3.* ***trace elements analyzed by XRF.*

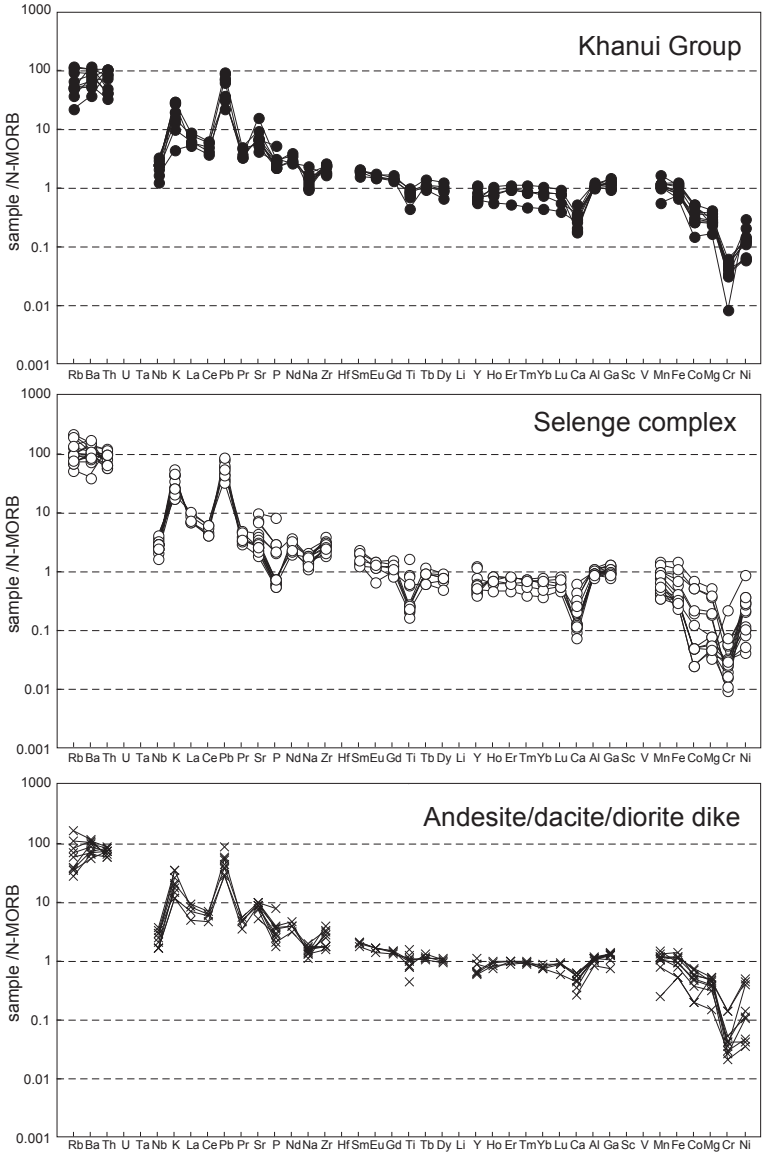

Fig. 5 MORB-normalized multi-element concentrations diagrams (spidergram) of the examined samples. Normalizing MORB composition by Sun and McDonough (1989) is used.

Magma type of the examined rocks

The geochemistry of igneous rocks gives evidence for the tectonic setting of the igneous activity that formed it because the chemical composition of igneous rocks varies according to its origins, and many diagrams for discrimination of igneous rocks have been proposed (e.g. Pearce, 1982). In this section, selective discrimination diagrams are used to discuss the magma type of the volcano-plutonic rocks in the Oyut-uul area.

The data from the Khanui Group, Selenge complex and dike make a liner trend together in the variation diagram, and therefore, they might have had same origin (Fig. 4). The spidergrams for the samples show geochemical characteristics similar to arc-related igneous rocks, such as enrichment of large-ion lithophile elements (LILE) in comparison to high-field-strength elements (HFSE) and REE with negative Nb anomaly (e.g. Pearce et al., 2005, Fig. 5). The most data are plotted in the calc-alkaline field in the SiO_2 vs. FeO*/MgO diagram (Miyashiro, 1974, Fig. 7). Taking these lines of evidence together, it is concluded that the examined rocks are of

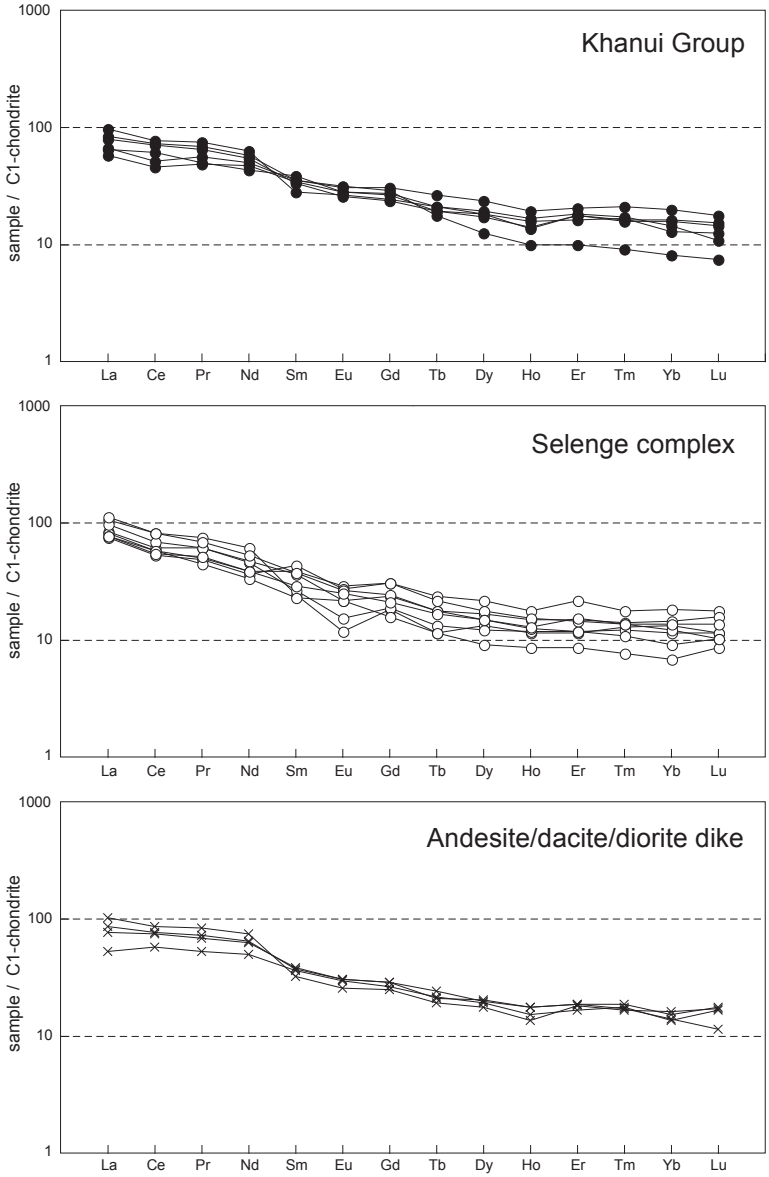

Fig. 6 Chondorite-normalized REE patterns of the examined samples. Normalizing chondrite values are after Sun and McDonough (1989).

calc-alkaline series formed at an arc environment. The samples have extremely high Sr concentration similar to the adakitic rocks (Table 1). The adakites are characterized by SiO_2 > 56 wt.%, Al_2O_3> 15 wt.%, Sr > 400 ppm, high Sr/Y ratio, and fractionated REE (e.g. Defant and Drummond, 1990; Drummond et al., 1996; Martin, 1999). The present samples, SiO_2 53–78 wt.% (avg. 66 wt.%), Al_2O_3 13–19 wt.% (avg. 16 wt.%), Sr 172–1470 ppm (avg. 557 ppm), Sr/Y 12–332 (avg. 41) and La/Yb 5–18 (avg. 10), likely have adakitic nature in this aspect.

It is suggested that typical adakitic magma is originated from partial melting of subducted oceanic slab at ca. 2.0 GPa and 900–950 ˚C (e.g. Defant and Drummond, 1990; Rapp, 1997; Sen and Dunn, 1994), and various processes during its rising up through mantle wedge and crust cause the diversity of adakites. Whereas, Atherton and Petford (1993) presented that the partial melting of newly under-plated basaltic crust should be considered as an alternative way of generating of adakites. Zhang et al. (2005) divided the adakites into the following two types based on

their origins: adakites derived from the partial melting of subducted oceanic slab (Type 1), and adakites derived from the partial melting of newly under-plated basaltic crust (Type 2). Distinct geochemical differences (K_2O and Al_2O_3contents, Mg#(=100 × Mg/(Mg+Fe)) and δ Sr values) between these types are recognized. Type 2 adakites, for example, generally have lower Al_2O_3concentration (less than ca. 16 wt.%) and higher K_2O/Na_2O ratio (ca. 0.5 or more) than Type 1 (Kamei et al., 2009; Liu et al., 2010; Zhang et al., 2005). The present samples, having high Al_2O_3 concentration (13–19 wt.%, avg. 16 wt.%) and low K_2O/Na_2O ratio (0.2 − 1.0, avg. 0.5), coincide with the type 1 which is derived from the oceanic slab-melt (Fig. 8). Therefore, it is likely that the rocks of the Oyut-uul were originated from a subducted slab-melt, from viewpoint of Al, Na, and K contents.

Spidergrams and REE chondrite-normalized patterns of the samples are similar to those of the marginal facies of the Kitakami adakitic granite of Japan (Tsuchiya et al., 2007, Fig. 9). The rocks are comparatively similar to

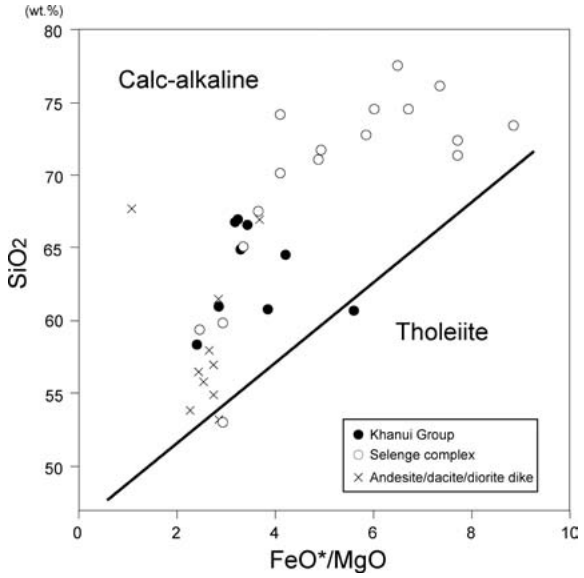

Fig. 7 Discrimination diagram of FeO*/MgO vs. SiO_2 (Miyashiro, 1974).

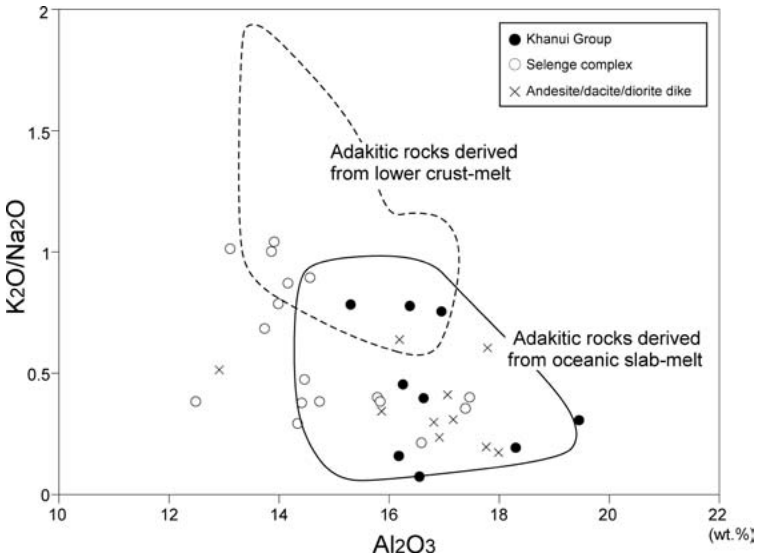

Fig. 8 K_2O/Na_2O vs. Al_2O_3 diagram (Kamei et al., 2009, 2013; Liu et al., 2010).

the marginal facies of the Kitakami adakitic granite also in having transitional characteristics between the adakite and island arc andesite/dacite/rhyolite in Sr/Y-Y relationship, and in having slightly higher MgO concentration than experimental slab-melt (Rapp and Watson, 1995; Sen and Dunn, 1994; Tsuchiya et al., 2007, Figs. 10 and 11). Tsuchiya et al. (2007) pointed out that the central facies of the Kitakami adakitic granite substantially represents

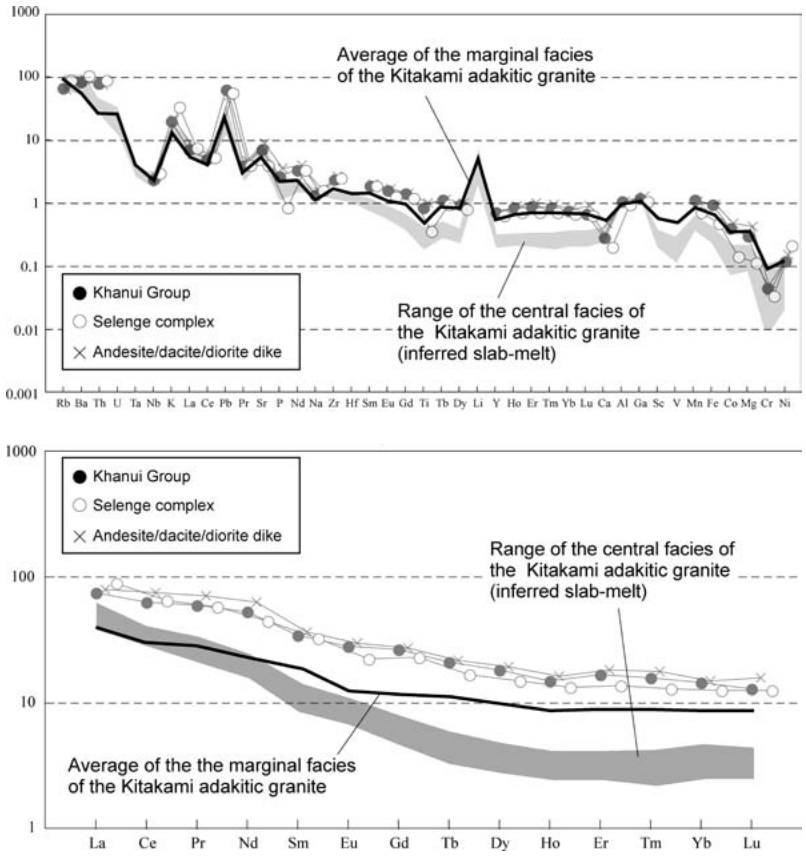

Fig. 9 MORB-normalized multi-element concentrations diagrams (a) and chondrite-normalized REE patterns (b) of the rocks from Oyut-uul area compared to the Kitakami adakitic granites. The data of the Kitakami adakitic granites are from Tsuchiya et al. (2007).

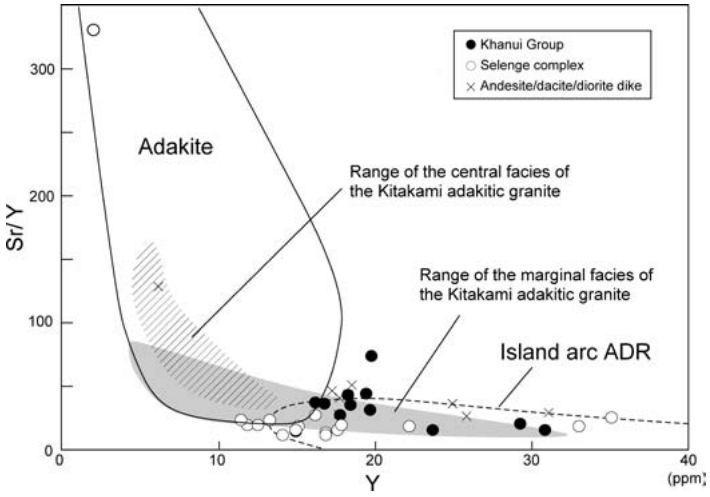

Fig. 10 Discrimination diagram of Sr/Y vs. Y. Adakite and Island arc ADR (andesite/dacite/rhyolite) fields are after Defant et al. (1991) and Martin et al. (2005). Ranges of the Kitakami adakitic granites are from Tsuchiya et al. (2007).

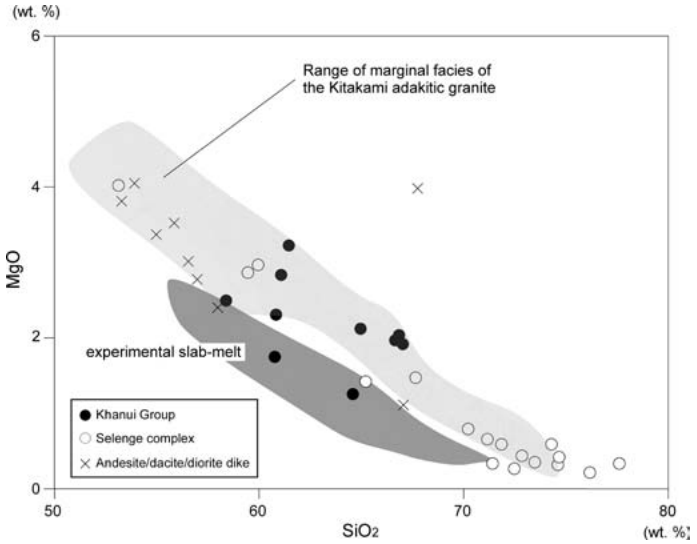

Fig. 11 Diagram of MgO vs. SiO_2. The range of marginal facies of the Kitakami adakitic granite is from Tsuchiya (2008). The field of the experimental slab-melt is after Rapp and Watson (1995) and Sen and Dunn (1994).

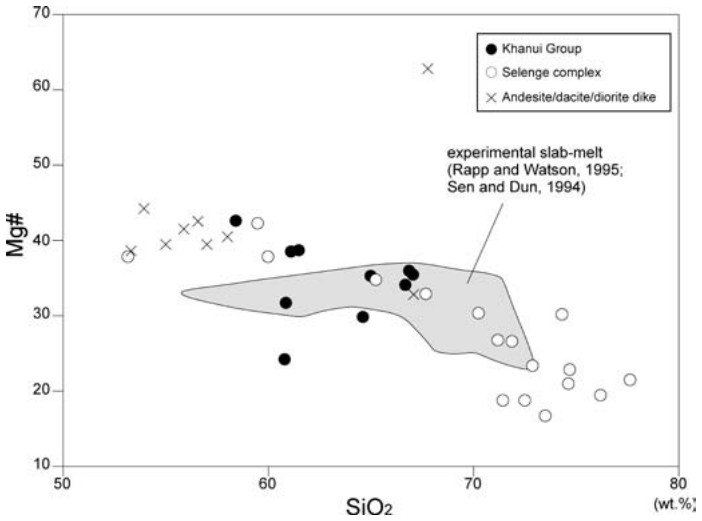

Fig. 12 Mg# vs. SiO_2 diagram. The field of the experimental slab-melt is after Rapp et al. (1991), Winther and Newton (1991), Sen and Dunn (1994), and Rapp and Watson (1995).

the primitive slab-melt composition, on the other hand, marginal facies of that was resulted from interaction between the slab-melt and mantle peridotite/lower crustal amphibolite during their ascent. Experimental petrology revealed that interaction with peridotite increases the Mg# in the melt generated by partial melting of mid-oceanic ridge basalt (e.g. Rapp et al., 1999). The samples, which have higher Mg# than experimental slab-melt, might imply that the initial magma of the Oyut-uul rocks derived from oceanic slab-melt had interacted with mantle peridotite (Fig. 12).

Summary

1. The examined rocks (lava of the Khanui Group, plutonic rock of the Selenge complex, and andesite/dacite/diorite dike) show a liner trend together in the variation diagram, and therefore, they might have had same origin.

2. The rocks are of calk-alkaline series formed at an arc environment.

3. The rocks have an adakitic nature derived from oceanic slab-melt.

4. The rocks are similar to the marginal facies of the Kitakami adakitic granite of Japan in having transitional characteristics between the adakite and island arc andesite/dacite/rhyolite in Sr/Y-Y relationship, and in having slightly higher MgO concentration than experimental slab-melt. Spidergram and REE chondrite-normalized pattern also suggest similarity between the present rocks and the marginal facies of the Kitakami granite.

5. The adakitic volcanic rock, derived from oceanic slab-melt, in the Sayan-Baikal belt presented in this paper gives concrete confirmation of the Late Paleozoic subduction of an oceanic plate beneath the "Siberian continent."

Acknowledgements

We would like to thank Profs. M. Takeuchi and H. Yoshida at Nagoya University for valuable comments. We appreciate critical review comments from an anonymous reviewer. Special thanks go to Mr. S. Yogo and Ms. M. Nozaki for their technical support.

References

Atherton, M. P. and Petford, N. (1993) Generation of sodium-rich magmas from newly underplated basaltic crust. *Nature*, **362**, 144–146.

Badarch, G., Cuninham, W. D., and Windley, B. F. (2002) A new terrane subdivision for Mongolia: Implications for the Phanerozoic crustal growth of central Asia. *Journal of Asian Earth Sciences*, **21**, 87–110.

Defant, M. J. and Drummond, M. S. (1990) Derivation of some modern arc magmas by melting of young subducted lithosphere. *Nature*, **347**, 662–665.

Defant, M. J., Richerson, P. M., DeBoer, J. Z., Stewart, R. H., Maury, R. C., Bellon, H., Drummond, M. S., Feigenson, M. D., Maury, R. C., and Jackson, T. E. (1991) Dacite genesis via both slab melting and differentiation: petrogenesis of La Yeguada volcanic complex, Panama. *Journal of Petrology*, **32**, 1101–1142.

Drummond, M. S., Defant, M. J., and Kepezhinskas, P. K. (1996) The petrogenesis of slab derived trondhjemite-tonalite-dacite/adakite magmas. *Transactions of the Royal Society of Edinburgh Earth Sciences*, **87**, 205–216.

Gerel, O. and Munkhtsengel, B. (2005) Erdenetiin Ovoo porphyry copper-molybdenum deposit in central Mongolia. Porter, T. M. (ed.), *Super Porphyry Copper & Gold Deposits – A Global Perspective v*. **2**, 525–543, PGC Publishing, Adelaide.

Gombosuren, S. and Batchuluun, P. (1994) *Oyut uul Geology Map / License #4947X*. "Tsogt-Tm" LLC., Ulaanbaatar. (In Mongolian)

Kamei, A., Miyake, Y., Owada, M., and Kimura, J.-I. (2009) A pseudo adakite derived frompartial melting of tonalitic to granodioritic crust, Kyushu, southwest Japan arc. *Lithos*, **112**, 615–625.

Kamei, A., Horie, K., Owada, M., Yuhara, M., Nakano, N., Osanai, Y., Adachi, T., Hara, Y., Terao, M., Teuchi, S., Shimura, T., Tsukada, K., Hokada, T., Iwata, C., Shiraishi, K., Ishizuka, H., and Takahash, Y. (2013) Late Proterozoic juvenile arc metatonalite and adakitic intrusions in the SørRondane Mountains, eastern Dronning Maud Land, Antarctica. *Precambrian Research*, **234**, 47–62.

Koval, P. V., Yakimov, V. M., Naigebauer, V. A., and Goreglyad, A. V. (1982) Late Mesozoic intrusive associations of Mongolia. Brief description and chemical composition. *Regional Petrochemistry of Mesozoic Intrusions of the Mongolia*. Nauka, **34**, 97–201. (In Russian)

Kovalenko, V. I., Yarmolyuk, V. V., Kovach, V. P., Kotov, A.B., Kozakov, I. K., Salnikova, E. B., and Larin, A. M. (2004) Isotope provinces, mechanisms of generation and sources of the continental crust in the Central Asian mobile belt:

geological and isotopic evidence. *Journal of Asian Earth Science*, **23**, 605–627.

Kurihara, T., Tsukada, K., Otoh, S., Kashiwagi, K., Minjin, C., Dorjsuren, B., Boijir, B., Sersmaa, G., Manchuk, N., Niwa, M., Tokiwa, T., Hikichi, G., and Kozuka, T. (2008) Upper Sillurian and Devonian pelagic deep-water radiolarian chert from the Khangai-Khentei belt of Central Mongolia: Evidence for Middle Paleozoic subduction-accretion activity in the Central Asian Orogenic Belt. *Journal of Asian Earth Sciences*, **34**, 209–225.

Liu, S.-A., Li, S., and He, Y., Huang, F. (2010) Geochemical contrasts between early Cretaceous ore-bearing and ore-barren high-Mg adakites in central-eastern China: implications for petrogenesis and Cu–Au mineralization. *Geochimica et Cosmochimica Acta*, **74**, 7160–7178.

Martin, H. (1999) Adakitic magmas: modern analogues of Archean granitoids. *Lithos*, **46**, 411–429.

Martin, H., Smithies, R. H., Rapp, R., Moyen, J.-E., and Charnpion, D. (2005) An overview of adakite, tonalite-trondbjcmitc-granodiorite (TTG) and sanukitoid: relationships and some implications for crustal evolution. *Lithos,* **79**, 1–24.

Miyashiro, A. (1974) Volcanic rock series in island arcs and active continental margins. *American Journal of Science*, **274**, 321–355.

Mossakovsky, A. A. and Tomurtogoo, O. (1976) *Upper Paleozoic of Mongolia*. Nauka, Moscow, 125p. (In Russian)

Munkhtsengel, B., Gerel, O., Tsuchiya, N. and Ohara, M. (2007) Petrochemistry of igneous rocks in area of the Erdenetiin Ovoo porphyry Cu-Mo mineralized district, northern Mongolia. Tohji, K., Tsuchiya, N. and Jeyadevan, B. (eds.), *Water Dynamics: 4th International Workshop on Water Dynamics*, 63–65, American Institute of Physics, New York.

Onon, G. (2017 MS) *Late Paleozoic Low-angle Southward-dipping Thrust in the Züünharaa Area, Mongolia: Implication for the Tectonic Process of the Central Asian Orogenic belt*. Dr. thesis of the Nagoya University, 50p. and 25 figs.

Onon, G. and Tsukada, K. (2017) Late Paleozoic low-angle southward-dipping thrust in the Züünharaa area, Mongolia: tectonic implications for the geological structures in the Sayan-Baikal and Hangai-Daur belts. *International Journal of Earth Science*, **106**, 2549–2573.

Pearce, J. A. (1982) Trace element characteristics of lavas from destructive plate boundaries. Thorpe, R. S. (ed.), *Andesites*, 528–548, John Wiley & Sons, Chichester.

Pearce, J. A., Stern, R. J., Bloomer, S. H., and Fryer, P. (2005) Geochemical Mapping of the Mariana Arc-Basin System: Implications for the Nature and Distribution of Subduction Components. *Geochemistry, Geophysics, Geosystems*, **6**, doi:10.1029/2004GC000895.

Petrov, O. V., Pospelov, I. I., and Shokalsky, S. P. (2014) Legend and tectonic zoning of Northern, Central and Eastern Asia (Central Asian fold belt and adjacent tectonic structures). Petrov, O. V., Leonov, Y. G., and Pospelov, I. I. (eds,), *Tectonics of Northern, Central and Eastern Asia. Explanatory Note to the Tectonic Map of Northern–Central–Eastern Asia and Adjacent Areas at Scale 1:2 500 000*, 18–32, VSEGEI Printing House.

Rapp, R. P. (1997) Heterogeneous source regions for Archean granitoids: experimental and geochemical evidence. Wit de M. J. and Ashwal L. D. (eds.), *Greenstone Belts*, 267-279, Oxford monographs on geology and geophysics v. 35, Clarendon Press, Oxford.

Rapp, R. P. and Watson, E. B. (1995) Dehydration melting of metabasalt at 8–32 kbar: implications for continental growth and crust–mantle recycling. *Journal of Petrology*, **36**, 891– 931.

Rapp, R. P., Watson, E. B., and Miller, C. F. (1991) Partial melting of amphibolite/eclogite and the origin of Archean trondhjemites and tonalites. *Precambrian Research*, **51**, 1–25.

Rapp, R. P., Shimizu, N., Norman, M. D., and Applegate, G. S. (1999) Reaction between slab-derived melts and peridotite in the mantle wedge: experimental constraints at 3.8 GPa. *Chemical Geology*, **160**, 335–356.

Sen, C. and Dunn, T. (1994) Dehydration melting of a basaltic composition amphibolite at 1.5 and 2.0 GPa: implications for the origin of adakites. *Contributions to Mineralogy and Petrology*, **117**, 394–409.

Sengör A. M. C., Natal' In B. A., and Burtman V. S. (1993) Evolution of the Altaid tectonic collage and Palaeozoic crustal growth in Eurasia. *Nature*, **364**, 299–307.

Sotnikov V. I., Berzina, A. N., Zhamsran, M., Garamzhav, D., and Bold, D. (1985) Copper deposits of Mongolia.

Transactions of the Joint Soviet-Mongolian Scientific-Research Expedition, Novosibirsk Nauka, **43**, 223. (In Russian)

Sun, S. S. and McDonough, W. F. (1989) Chemical and isotopic systematics of oceanic basalts: implications for mantle composition and processes. Saunders, A. D. and Norry, M. J. (eds.), *Magmatism in the Ocean Basins*, 313–345. Special publication of geological society of London, **42**.

Takebe, M. and Yamamoto, K. (2003) Geochemical fractionation between porcellanite and host sediment. *Journal of Geology*, **111**, 301–312.

Takeuchi, M., Tsukada, K., Suzuki, T., Nakane, Y., Sersmaa, G., Manchuk, N., Kondo, T., Matsuzawa, N., Bakhat, N., Khishigsuren, S., Onon, G., Katsurada, Y., Hashimoto, M., Yamasaki, S., Matsumoto, A., Oyu-Erdene, B., Bulgantsengel, M., Kundyz, S., Enkhchimeg, L., Ganzorig, R., Myagmarsuren, G., Jamiyandagva, O., and Molomjamts, M. (2012) Stratigraphy and geological structure of the Paleozoic system around Ulaanbaatar, *Mongolia. Bulletin of the Nagoya University Museum*, **28**, 1–18.

Tomurtogoo, O. (2003) *Tectonic Map of Mongolia at the Scale of 1:1 000000 and Tectonics of Mongolia (Brief Explanatory Notes of the Map)*. Mineral Resources Authority of Mongolia, Ulaanbaatar.

Tsuchiya, N. (2008) Petrogenes of adakites and their geological significance. *Earth Science (Chikyu Kagaku)*, **62**, 161–182. (In Japanese)

Tsuchiya, N., Kimura, J. I., and Kagami, H. (2007) Petrogenesis of Early Cretaceous adakitic granites from the Kitakami Mountains, *Japan. Journal of Volcanology and Geothermal Research*, **167**, 134–159.

Tsukada, K., Nakane, Y., Yamamoto, K., Kurihara, T., Otoh, S., Kashiwagi, K., Minjin, Ch., Sersmaa, G., Manchuk, N., Niwa, M., and Tokiwa, T. (2013) Geological setting of basaltic rocks in an accretionary complex, Khangai–Khentei belt, Mongolia. *Island Arc*, **22**, 227–241.

Winther, K. T. and Newton, R. C. (1991) Experimental melting of hydrous low K tholelite: evidence on the origin of Archean cratons. *Bulletin of Geological Society of Denmark*, **39**, 213–228.

Yamamoto, K. and Morishita, T. (1997) Preparation of standard composites for the trace element analysis by X-ray fluorescence. *Journal of Geological Society of Japan*, **103**, 37–45. (In Japanese)

Yamamoto, K., Yamashita, F. and Adachi, M. (2005) Precise determination of REE for sedimentary reference rocks issued by the Geological Survey of Japan. *Geochemical Journal*, **39**, 289-297.

Zhang, H. X., Niu, H. C., Sato, H., Yu, X. Y., Shan, Q., Zhang, B., Ito, J., and Nagao, T. (2005) Late Paleozoic adakites and Nb-enriched basalts from northern Xinjiang, northwest China: Evidence for the southward subduction of the Paleo-Asia Oceanic Plate. *Island Arc*, **14**, 55–68.